Interligand Overhauser Effects in Type II Dihydrofolate Reductase

Dawei Li,[‡] Louis A. Levy,[‡] Scott A. Gabel,[‡] Mark S. Lebetkin,[‡] Eugene F. DeRose,[‡] Mark J. Wall,[§] Elizabeth E. Howell,[||] and Robert E. London*,[‡]

Laboratory of Structural Biology, MR-01, National Institute of Environmental and Health Sciences, Box 12233, Research Triangle Park, North Carolina 27709, Department of Chemistry, The Pennsylvania State University, University Park, Pennsylvania 16802, and Biochemistry, Cell and Molecular Biology Department, F327B Walters Life Sciences, University of Tennessee−Knoxville, Knoxville, Tennessee 37996

Received November 16, 2000; Revised Manuscript Received February 6, 2001

ABSTRACT: R67 dihydrofolate reductase (DHFR) is a type II DHFR produced by bacteria as a resistance mechanism to the increased clinical use of the antibacterial drug trimethoprim. Type II DHFRs are not homologous in either sequence or structure with chromosomal DHFRs. The type II enzymes contain four identical subunits which form a homotetramer containing a single active site pore accessible from either end. Although the crystal structure of the complex of R67 DHFR with folate has been reported [Narayana et al. (1995) *Nat. Struct. Biol. 2,* 1018], the nature of the ternary complex which must form with substrate and cofactor is unclear. We have performed transferred NOE and interligand NOE (ILOE) studies to analyze the ternary complexes formed from $NADP^+$ and folate in order to probe the structure of the ternary complex. Consistent with previous studies of the binary complex formed from another type II DHFR, the ribonicotinamide bond of $NADP^+$ was found to adopt a syn conformation, while the adenosine moiety adopts an anti conformation. Large ILOE peaks connecting $NADP^+$ H4 and H5 with folate H9 protons are observed, while the absence of a large ILOE connecting $NADP^+$ H4 and H5 with folate H7 indicates that the relative orientation of the two ligands differs significantly from the orientation in the chromosomal enzyme. To obtain more detailed insight, we prepared and studied the folate analogue 2-*d*eamino-2-*m*ethyl-5,8-*did*eaza*f*olate (DMDDF) which contains additional protons in order to provide additional NOEs. For this analogue, the exchange characteristics of the corresponding ternary complex were considerably poorer, and it was necessary to utilize higher enzyme concentrations and higher temperature in order to obtain ILOE information. The results support a structure in which the $NADP^+$ and folate/DMDDF molecules extend in opposite directions parallel to the long axis of the pore, with the nicotinamide and pterin ring systems approximately stacked at the center. Such a structure leads to a ternary complex which is in many respects similar to the gas-phase theoretical calculations of the dihydrofolate−NADPH transition state by Andres et al. [(1996) *Bioorg. Chem. 24,* 10−18]. Analogous NMR studies performed on folate, DMDDF, and R67 DHFR indicate formation of a ternary complex in which two symmetry-related binding sites are occupied by folate and DMDDF.

Dihydrofolate reductase (DHFR)[1] catalyzes the NADPH-dependent reduction of dihydrofolate to tetrahydrofolate, thereby providing a critical cofactor for one-carbon metabolism. Chromosomal DHFRs have been important targets for antifolate agents, directed against both the human (e.g., methotrexate) and bacterial (e.g., trimethoprim) enzymes. The emergence of bacteria resistant to trimethoprim and related drugs was found in some cases to result from the presence of a resistance plasmid coding for a type II DHFR, which is structurally and evolutionarily unrelated to the extensively studied chromosomal DHFRs (*1*−*4*). In particular, the bacterial enzyme is a 78 amino acid peptide which forms a compact β-barrel structure and assembles to form a tetramer, creating an active site pore which binds both substrate and cofactor (*5*). Despite these structural differences, both the type I and type II enzymes have been shown to transfer the *pro-R* hydrogen on the A side of the nicotinamide ring of NADPH stereospecifically to the *re* face of the pteridine ring of dihydrofolate (*6*, *7*).

Although the crystal structure of a truncated form of the protein, lacking a disordered N-terminal 16 amino acid peptide, has been determined to 1.7 Å resolution (*5*), structural information on the interaction of the enzyme with substrates and cofactors is, at this point, fairly limited. This is due to the 222 symmetry associated with the structure. When a ligand binds to an active site possessing 222 symmetry, it has four symmetry-related sites from which to choose. If these sites are not fully occupied due to steric constraints, symmetry is preserved by random packing of the ligands in the binding sites, resulting in electron density

* To whom correspondence should be addressed. Phone: 919-541-4879. Fax: 919-541-5707. E-mail: london@niehs.nih.gov.

[‡] National Institute of Environmental and Health Sciences.

[§] The Pennsylvania State University.

[||] University of Tennessee−Knoxville.

[1] Abbreviations: DMDDF, 2-deamino-2-methyl-5,8-dideazafolate (DMDDF); DHFR, dihydrofolate reductase; ILOE, interligand Overhauser effect; ITC, isothermal titration calorimetry; $NADP^+$, nicotinamide adenine dinucleotide phosphate; NMN, nicotinamide mononucleotide; NMR, nuclear magnetic resonance; NOE, nuclear Overhauser effect.

10.1021/bi0026425 CCC: $20.00
Published on Web 03/16/2001

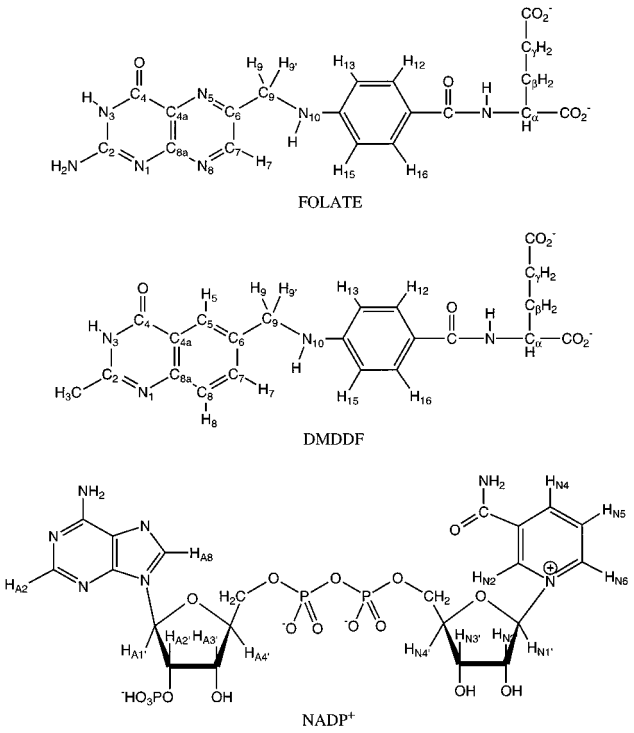

FIGURE 1: Numbering of nuclei in folate, $NADP^+$, and the folate analogue DMDDF. $NADP^+$ protons are referred to by the subscripts shown in the figure, e.g., N2 corresponds to the proton on C-2 of nicotinamide, etc. Folate protons are denoted as Fi, where i corresponds to the number in the figure, and the protons of the *f*olate *a*nalog DMDDF are referred to as FAi. The protons on the methyl group at the C-2 position of the folate analogue are referred to as FA2.

with partial occupancy. This situation is observed for the folate−R67 DHFR complex. Isothermal titration calorimetry (ITC) studies have demonstrated that R67 DHFR can form a variety of ternary complexes, not only involving the catalytically active NADPH + dihydrofolate ligands but involving pairs of folate or NADPH ligands as well (*8*).

Interligand Overhauser effects (ILOEs) provide a powerful method for studying the structure of ternary complexes formed by pairs of small molecules interacting with macromolecular receptors (*9*−*11*). NOE interactions formed in the ternary complex are transferred to the pair of uncomplexed ligands due to chemical exchange, offering the same advantages of analysis on high concentrations of small molecules as in the more typical transferred NOE experiment performed on binary complexes. In the present study, we have used interligand Overhauser effects to characterize the structure of several ternary complexes formed between R67 DHFR and the ligands $NADP^+$ and folate as well as the folate analogue 2-deamino-2-methyl-5,8-dideazafolate (DMDDF). The latter folate analogue was selected due to the presence of additional protons which can provide NOE information useful for orienting the bound ligand. The present studies demonstrate an ILOE pattern which is inconsistent with the previously modeled structure which was based on the complex formed with the chromosomal DHFR (*5*) and provide strong evidence that the pairs of molecules identified from the ITC studies bind from opposite ends of the active site pore such that the reactive pterin or pyridine rings meet at the center.

METHODS

Type II DHFR was prepared as described previously (*12*). The enzyme was lyophilized and subsequently redissolved in buffer for each study. $NADP^+$, folate, and *N*-(4-aminobenzoyl)-L-glutamic acid diethyl ester were obtained from Sigma and used without additional purification. The perdeuterated Tris-d_{11} buffer was obtained from Isotec, Inc. (Miamisburg, OH).

The folate analogue 2-*d*eaza-2-*m*ethyl-5,8-*did*eaza*f*olate (DMDDF) (Figure 1) was synthesized essentially as described by Hughes et al. (*13*). The precursor 2,6-dimethyl-3,4-dihydro-4-oxoquinazoline was prepared as described by Sen and Gupta (*14*). The 6-methyl group was selectively brominated with *N*-bromosuccinimide (NBS). We note, however, that, in contrast to ref *13*, we found that the brominated derivative produced was present in the chloroform solution along with some unreacted starting material. The precipitate formed and reported as the desired product was found to be the hydrobromide salt of the starting material. After washing the organic layer, drying, and removal of the solvent, the mixture obtained was used in the next step. Diethyl *N*-[4-(*N*-(3,4-dihydro-2-methyl-4-oxo-6-quinazolinyl)methyl]aminobenzoyl]-L-glutamate was prepared by reaction with commercial *N*-(4-aminobenzoyl)-L-glutamic acid diethyl ester with a slightly altered workup. After overnight reaction at 80 °C, the reaction mixture was poured into ice water. The aqueous mixture was extracted three times with ethyl acetate, which served to remove the excess glutamate derivative starting material, and then with ether (four times). The ether extract was washed with water and dried, and the solvent was removed to yield an oil which crystallized upon trituration with ethyl acetate. The ester was hydrolyzed with aqueous 1 N NaOH as described by Hughes et al. (*13*).

The NMR samples were prepared by mixing stock solutions of R67 DHFR and ligands in D_2O containing 100 mM Tris-d_{11} buffer at pH 8.0 or 9.0. The total protein concentration used was 0.1 or 0.5 mM (expressed as a tetramer), as indicated. Ligands were typically present at 5 mM concentrations, unless otherwise indicated. All proton NMR measurements were performed at 500 MHz on a Varian UNITYplus 500 NMR spectrometer at 20 or 35 °C, using a Nalorac 5 mm triple resonance probe. Phase-sensitive NOESY spectra were acquired, with spectral widths of 12.0 ppm. F_1 quadrature detection was achieved via the States−TPPI method (*15*). The data were acquired as a 256 (t_1) × 512 (t_2) complex matrix, with a 2.5 s recovery delay between scans. Sixteen or 32 scans were acquired per t_1 increment, resulting in total acquisition times of ∼7 or 14 h, when the mixing time was set to 0.5 s. The residual HOD signal was suppressed using presaturation via CW irradiation, with a field strength of ∼50 Hz, applied for 0.5 s during the recovery delay and during the entire mixing time. The data were processed with NMRPipe (*16*). The time domain data were multiplied by cosine-squared bell functions in each dimension and zero filled, resulting in a final matrix size of 512 (F_1) × 1024 (F_2) after Fourier transformation. Cross-peak volumes were measured using SPARKY (*17*).

RESULTS

NOE data were collected on the nonproductive ternary complex formed from 5 mM $NADP^+$, 5 mM folate (see

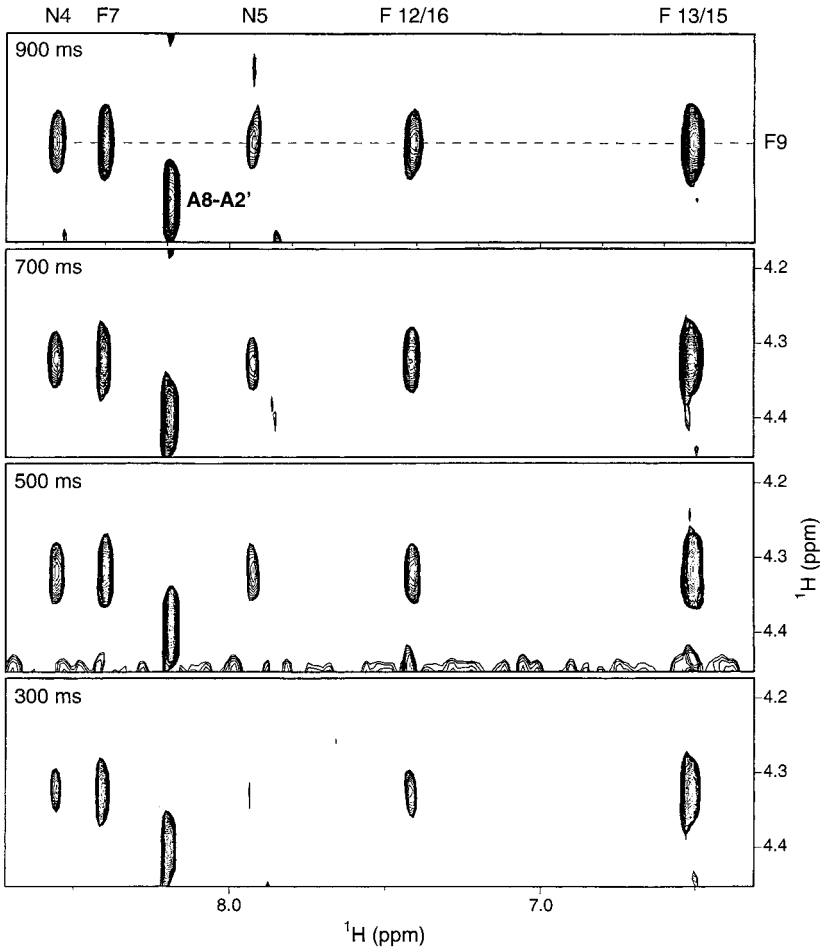

FIGURE 2: A portion of NOESY spectra illustrating the cross-peaks connecting the folate H-9 protons with the aromatic protons of folate and $NADP^+$, obtained on a sample containing 5 mM folate, 5 mM $NADP^+$, and 0.1 mM R67 DHFR in a 100 mM Tris-d_{11}, pH 8.0, and D_2O buffer. The spectra correspond to mixing times of 300, 500, 700, and 900 ms, as indicated.

Figure 1 for numbering), and type II DHFR (0.1 mM tetramer concentration) prepared in a D_2O buffer (100 mM Tris-d_{11}; pH 8, uncorrected meter reading). Studies were performed at pH 8 in order to maintain the enzyme in its active form as a tetramer, since the enzyme undergoes a pH-dependent reversible dissociation to a dimer characterized by a pK = 6.84 (*18*). Examination of the NOESY spectra as a function of mixing time for this complex showed strong interligand peaks connecting the folate C-9 methylene protons and the $NADP^+$ pyridine H4 and H5 protons. A series of NOESY spectra corresponding to the aromatic region of the spectrum and showing the cross-peaks with the folate H-9 protons obtained at mixing times of 300, 500, 700, and 900 ms are shown in Figure 2, and curves showing the time development of the corresponding ILOE peaks are shown in Figure 3A. In addition to these strong interligand NOEs, relatively weak interligand peaks connecting the $NADP^+$ N4 and N5 protons with F13/15 and the $NADP^+$ N1′ with F7 were also observed, where we have followed the numbering convention shown in Figure 1. In the latter cases, there is a pronounced lag in the development of the ILOE, which suggests that there may be significant indirect dipolar relaxation pathways involved. For the interaction involving the *p*-aminobenzoyl protons there is an obvious possible spin diffusion pathway through the folate: N4/5−F9−F13/15, which is consistent with the large F9−F13/15 transferred NOE interaction which can be observed.

As discussed previously (*10*), ILOE studies typically require longer mixing times than transferred NOE studies due to the longer internuclear distances involved and the $1/r^6$ dependence of the interaction. The dependence of the NOE peaks on mixing time and particularly the spectrum obtained at a mixing time of 300 ms demonstrate the greater proximity of N4 than N5 to the F9 proton(s). The quantitation of interligand distances is complex and subject to a number of limitations. In the present case, the use of a reference distance for ILOE data becomes even more problematic, since the sample may in principle contain a mixture of binary $NADP^+$−DHFR as well as ternary $NADP^+$−folate−DHFR and $(folate)_2$−DHFR species. On the basis of the average slope of the build-up curves for N4−N5, N5−N6, and F12/16−F13/15, using the standard formula:

$$\frac{r_{ij}}{r_{kl}} = \left(\frac{\mathrm{NOE}_{kl}}{\mathrm{NOE}_{ij}}\right)^{1/6}$$

where NOE_{ij} corresponds to the initial slope of the NOE build-up curve between nuclei i and j, we obtained r_{N4-F9} = 4.1 Å and r_{N5-F9} = 5.0 Å, as summarized in Table 1. Clearly, given the inherent limitations and the fact that there are two F9 protons which must have different distances to the nicotinamide protons, this is a fairly qualitative measure.

In addition to the interligand Overhauser effects observed, many negative intraligand transferred NOE peaks are ob-

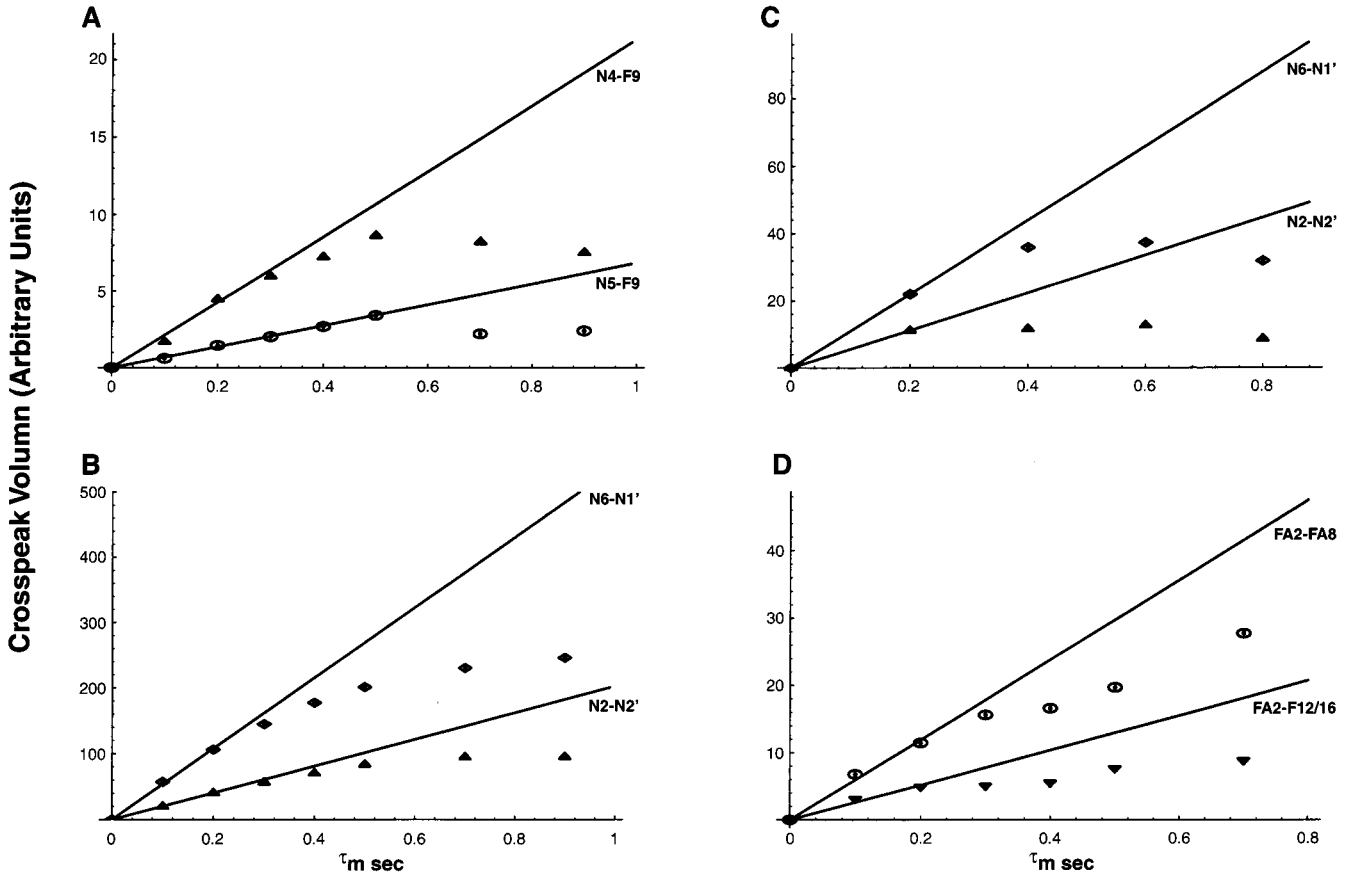

FIGURE 3: NOE build-up curves corresponding to (A) the interligand Overhauser interactions of N4−F9 (△) and N5−F9 (○) and (B) the intraligand interactions of $NADP^+$ N6−N1′ (◊) and N2−N2′ (△) in a sample containing 5 mM folate, 5 mM $NADP^+$, and 0.1 mM DHFR at 20 °C and pH 8.0. NOE build-up curves corresponding to (C) the intraligand interactions of $NADP^+$ N6−N1′ (◊) and N2−N2′ (△) in a sample containing 4 mM DMDDF, 4 mM $NADP^+$, and 0.5 mM DHFR at 35 °C and pH 8.0. (D) NOE interactions between the methyl protons of DMDDF and the DMDDF H-8 proton, FA2−FA8 (○), or the folate H13/15 protons, FA2−FA12/16 (▽), in a sample containing 5 mM folate, 5 mM DMDDF, and 0.1 mM DHFR at 20 °C and pH 9.0. The latter is an interligand NOE, while the former can have both intra- and interligand contributions, but is probably dominated by the former, as discussed in the text.

Table 1: Internuclear Distances Derived from Transferred NOE Experiments[a]

	complex		
spin pair	$NADP^+$−folate	$NADP^+$−DMDDF	fol−DMDDF
N6−N1′	2.2	2.4	
N2−N2′	2.6	2.7	
A8−A1′	4.2		
A8−A2′	2.8		
F7−F9	3.6	3.0	
N4−F9	4.1	3.8	
N5−F9	5.0		
N4−F7		3.6[b]	
N4−FA5		3.6	
N5−FA5		3.0	
N6−FA5		3.1	
F12−FA2			5.4
F13−FA2			5.4
F7−FA2			6.6

[a] Distances given in angstroms. [b] The N4−F7 distance is based on a few ILOE cross-peaks observed at longer mixing times.

served for both folate and $NADP^+$. Of particular interest are the large transferred NOE peaks connecting nicotinamide N6 with N1′ and N2 with N2′, as well as the adenosine A8 with A2′ (Figure 3, Table 1). This pattern establishes the glycosidic bond angles of $NADP^+$ in the ternary complex as syn for the ribonicotinamide moiety and anti for the adenosine. These results are in excellent agreement with previous transferred NOE studies of the binary complex formed by $NADP^+$ and the related R388 plasmid DHFR (*19*). On the basis of initial slopes of the NOE build-up curves for $NOE_{A8-A1'}/NOE_{A8-A2'}$, a distance ratio $r_{A8-A2'}/r_{A8-A1'} = 0.64$ is obtained. The calculated ratio $r_{A8-A2'}/r_{A8-A1'}$ obtained for adenosine as a function of the glycosidic bond angle for a 2′-endo conformation of the ribose was found to vary between 0.57 and 1.77, with the former value corresponding to the high anti range, i.e., close to −94°. Hence, the 0.64 ratio observed corresponds to a χ value close to the value of $\chi = -92 \pm 32°$ determined for the adenosyl group in $NADP^+$ in the R388 DHFR study. Negative transferred NOE peaks connecting the folate F7, F9, F12/16, and F13/15 protons are also observed. In contrast, the NOE peaks observed for the glutamate moiety of the folate were found to be positive (i.e., opposite in sign to the diagonal peaks). This result indicates that the folyl glutamate moiety does not have a well-defined binding orientation in the complex but continues to be characterized by rapid internal motion (i.e., $\tau_c < 1.12/\omega \sim 0.36$ ns) even in the ternary complex.

In control NOE studies performed in the absence of enzyme, we found that while the NOEs for the $NADP^+$ become positive, characteristic of a molecule whose motion falls into the extreme narrowing limit, the folate NOEs remained negative. This behavior is consistent with the

formation of large aggregates, which has been described previously (*20*, *21*). Lam and Kotowycz (*20*) suggested that the aggregates involve stacking interactions between approximately coplanar *p*-aminobenzoyl and pterin ring systems, such that the pterin ring of one folate is in close proximity with the *p*-aminbenzoyl rings of the adjacent folate molecules, and with alternate anionic glutamyl groups facing in opposite directions. According to Poe (*21*), the dissociation constants for dimerization were determined to be 1.4 mM for the "neutral" form (pterin ring uncharged) and 340 mM for the anionic form (pterin ring negatively charged). Consistent with the folate p*K* of 8.38 (*21*), we found that NOE studies on a 5 mM folate solution at pH 9 showed only positive NOEs. Hence, at pH 9 aggregation effects are negligible so that negative NOE values can be used as an indicator of enzyme binding.

The existence of folate aggregates can interfere with the transferred NOE experiments on folate performed below pH 9 to an extent which is dependent on the size of the aggregates and hence the degree to which cross-relaxation in the aggregate is competitive with cross-relaxation in the enzyme complex. To obtain more insight into the question of how ligand aggregation might affect transferred NOE and ILOE experiments, we performed additional theoretical calculations using the model system of two ligands of three spins each described elsewhere (*11*). The (isotropic) rotational correlation time for one of the ligands was set at 10^{-8} s to simulate the effect of aggregation. The results lead to several qualitative conclusions: (1) Initial slopes of transferred NOE peaks can be subject to significant errors due to aggregation of nominally free ligands leading to longer effective correlation times; such aggregation will weight the contributions of the ligand conformation in the aggregate more heavily relative to the contributions of the receptor-complexed ligand. (2) Initial slopes of the ILOE curves arising from direct interactions between spins on different ligands are not significantly perturbed by such aggregation. (3) Spin diffusion can occur in large aggregates, analogous to the behavior for the receptor-complexed ligand. NOE curves which involve relaxation mediated by spins in the aggregated ligand may be affected by aggregation. In general, such curves are still characterized by a lag or sigmoidal development of the NOE, while the slope of the curve after the initial lag period can be increased. In general, these results confirm the general conclusion that ILOE data are less subject to various sources of error than typical transferred NOE data obtained in studies of binary complexes. A comparison of the ILOEs observed at pH 8 and 9 indicates that there are no significant differences, while $NADP^+$ tends to be less stable at higher pH (*22*). Hence this does not appear to constitute a limitation for the analysis of ILOE data in this system.

Studies of the Folate Analogue, DMDDF. Due to the paucity of protons on the pterin ring, we prepared the analogue 2-deamino-2-methyl-5,8-dideazafolate (DMDDF) (Figure 1), which offers the possibility of additional NOE interactions involving protons at positions 2, 5, and 8. Unexpectedly, samples prepared analogously to the $NADP^+$−folate−DHFR solutions showed no apparent evidence supporting formation of this ternary complex. For this sample, the NOE resonances for $NADP^+$ were positive, while those for DMDDF were negative. Since it has been demonstrated that R67 DHFR can bind two folate molecules in a strongly cooperative manner ($K_{D1} = 390\ \mu M$; $K_{D2} = 24\ \mu M$) (*8*), the most probable interpretation of these results is that the degree of positive cooperativity for DMDDF binding with DHFR is increased relative to folate, and/or the degree of positive cooperativity for DMDDF−$NADP^+$ binding is decreased relative to folate−$NADP^+$. Thus, under the conditions of the study, we are observing transferred NOEs corresponding to the $DMDDF_2$−DHFR ternary complex but a negligible contribution from an $NADP^+$−DMDDF−DHFR ternary complex, which apparently is not forming to any significant degree. Further, the observation of negative transferred NOE cross-peaks indicates that although the stability of the ternary $(DMDDF)_2$−DHFR complex may be increased relative to the $(folate)_2$−DHFR complex, the K_{D2} value is probably ~1 μM or greater.

We subsequently attempted to obtain more information for this complex by increasing the enzyme concentration to 0.5 mM (tetramer) and then increasing the temperature to 35 °C. In combination, these changes allowed a sufficient degree of $NADP^+$ binding to result in negative transferred NOE peaks and allowed the observation of a number of interligand cross-peaks as well. For the $NADP^+$−DMDDF−DHFR complex observed under these conditions, we are able to observe analogous cross-peaks connecting N4 and N5 with the H-9 protons of DMDDF (also referred to as FA for folate analogue). Additional ILOE peaks connecting the FA5 with N4, N5, and N6 are also observed. Although ILOE peaks connecting N4 with FA7 are not observed at shorter mixing times, consistent with the observations in the $NADP^+$−folate−DHFR ternary complex, we did observe such peaks at mixing times greater than 0.5 s, and a derived distance is included in Table 1. This interaction may include indirect relaxation pathways; however, the proximity of N4 to FA9 suggests that a direct interaction between N4 and FA7 is not unreasonable.

Intraligand transferred NOE peaks observed for the $NADP^+$, particularly for N6−N1′ and N2−N2′ (Figure 3C), indicate that the $NADP^+$ binding to the ternary complex has a similar syn conformation of the ribonicotinamide glycosidic bond, supporting the conclusion that the ternary complex formed is structurally analogous to the $NADP^+$−folate−DHFR complex. Subject to the assumptions noted previously, several intra- and interligand distances derived from the transferred NOE measurements are summarized in Table 1. We note, however, that at the higher temperature used for this experiment there was significant degradation of the $NADP^+$ during the course of the study, resulting in considerably greater scatter for the NOE build-up curves, particularly corresponding to the weaker, longer distance interactions. This is undoubtedly one of the reasons for the greater dropoff of the NOE build-up curves shown in Figure 3C.

Interactions involving the methyl group of DMDDF, FA2, are potentially of considerable value for the characterization of the ternary $NADP^+$−DMDDF−DHFR complex. In the aromatic region of the spectra, we observed two cross-peaks: an intraligand peak between the C-2 methyl protons (FA2) and FA8, the closest proton in the DMDDF, and an apparent interligand peak between FA2 and the nicotinamide N2 proton (Figure 4). These resonances are observed only at the longest mixing times, >700 ms. More intense NOE peaks are observed upfield between FA2 and protons in the

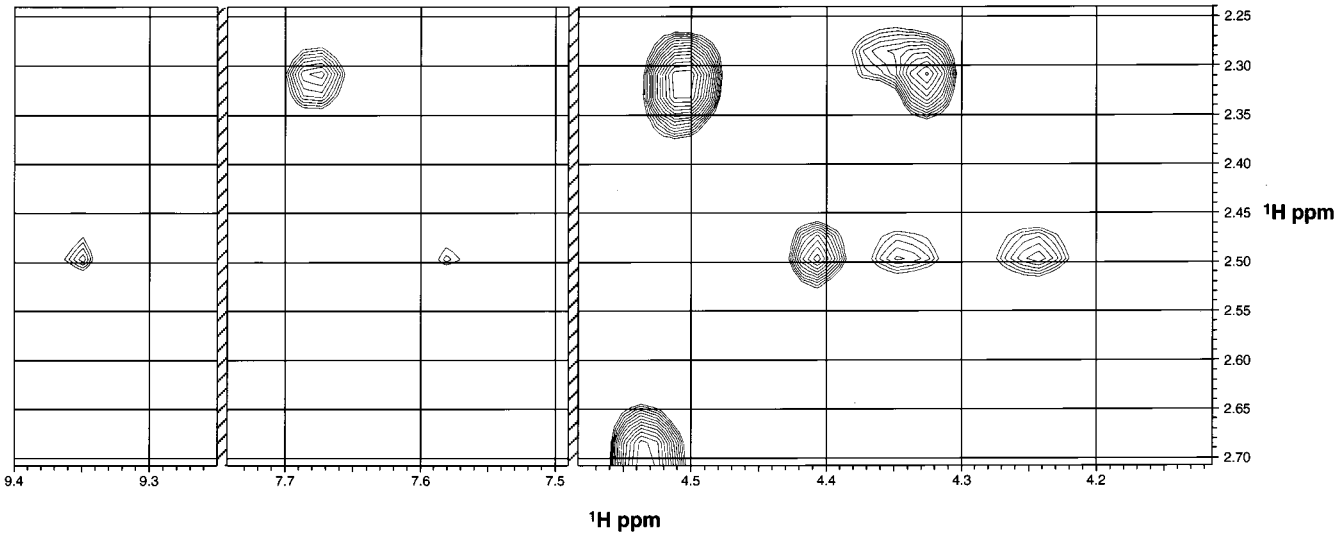

FIGURE 4: Portion of the NOESY spectrum showing cross-peaks involving the methyl protons of DMDDF which resonate at 2.5 ppm with resonances at 9.35 ppm ($NADP^+$ N2), 7.58 (DMDDF H-8), and ~4.2−4.5 ppm (ribose protons). The spectrum was obtained at $\tau_m = 700$ ms on a sample containing 4 mM $NADP^+$, 4 mM DMDDF, and 0.5 mM DHFR at 35 °C.

range 4.2−4.5 ppm (Figure 4). The latter correspond to ribose protons but could not be unambiguously assigned due to the congestion of resonances in this part of the spectrum. The data support the conclusion that, in the ternary complex, the methyl group of DMDDF is close to at least one of the ribosyl protons of the $NADP^+$.

The Folate−DMDDF−DHFR Complex. Since, as noted above, NOE studies on folate solutions at pH 8 yielded negative NOE values indicative of extensive aggregation, we investigated a solution containing 5 mM folate + 5 mM DMDDF but no enzyme. At pH 8, both folate and DMDDF exhibited negative NOE values consistent with aggregation. As the temperature was increased, the NOE values for DMDDF protons became positive and, at somewhat higher temperature, so did the NOE values for folate. A pH titration study of DMDDF indicated a p*K* for the quinazolone ring system of 10.51, considerably higher than the folate p*K*. Thus, although DMDDF might be expected to have a greater tendency to aggregate correlated with its higher p*K* value, the NOE data indicate that the reverse is true. As in the study of $NADP^+$ + folate discussed above, at pH 9 all NOEs are positive, indicating that at this pH aggregation is not a significant problem. Since even the DMDDF NOE values become positive, this result suggests that the aggregates observed at lower pH arise from mixed structures containing both folate and DMDDF. Interestingly, no specific folate−DMDDF cross-peaks could be observed in any of these studies. This result is consistent with the general conclusion that ILOE interactions will be less subject to errors resulting from aggregation than transferred NOE data.

The structure of the ternary complex involving the DMDDF analogue was evaluated by NOE studies performed at pH 9 on a sample made up of 5 mM folate, 5 mM DMDDF, and 0.1 mM DHFR. For this system, we observed significant, negative ILOEs between the methyl resonance of the DMDDF and the *p*-aminobenzoyl protons of folate, as well as a very weak ILOE connecting the DMDDF methyl protons with folate H7 (Figures 3D and 5). In this study, the higher pH value of 9 not only was useful for reducing aggregation but also resulted in a significant perturbation of the folate *p*-aminobenzoyl proton shifts so that it became possible to resolve the resonances arising from the *p*-aminobenzoyl groups of folate and DMDDF (Figure 5). The cross-peaks connecting FA2 with the *p*-aminobenzoyl protons apparent in Figure 5 may arise from analogous interligand interactions in the ternary $(DMDDF)_2$−DHFR species, as well as from intraligand interactions in one of the ternary complexes. Since at this pH we do not expect contributions from folate or mixed folate−DMDDF aggregates, these results indicate that in the folate−DMDDF−DHFR complex there must be substantial overlap of the pterin rings, yielding a structure qualitatively analogous to the folate aggregates observed in solution. NOE build-up curves comparing the FA2−F13/15 data with the FA2−FA8 data are shown in Figure 3D. As discussed above, the latter NOE can arise due to a combination of intra- and interligand interactions. Referencing the data to the fixed $r_{FA7-FA8} = 2.5$ Å, the $r_{FA2-FA8}$ distance is calculated as 5.3 Å, close to the expected intramolecular distance. This suggests a dominant contribution from the intramolecular relaxation pathway. The interligand r_{FA2-F7} distance is calculated to be 6.6 Å, somewhat longer than the corresponding distances between the folate C2 amino groups and F7 on the second, symmetry-related folate illustrated in the crystal structure (*5*).

Studies Using Other Folate Analogues. The different kinetic and stability behavior of the ternary $NADP^+$−folate−DHFR and $NADP^+$−DMDDF−DHFR complexes can in principle result from any of the modifications at positions 2, 5, or 8. To further explore the basis for these differences, we performed studies using either 5,8-dideazafolate or 8-deazafolate in the presence of $NADP^+$ and R67 DHFR. The complex formed using 5,8-dideazafolate behaved similarly to the complex formed using DMDDF, in particular showing little evidence for $NADP^+$ binding at 25 °C. In contrast, the complex formed using 8-deazafolate behaved more like the corresponding folate complex. These results indicate that the substitution at the 5 position of folate has a significant effect on stability and cooperativity of binding. According to the crystal structure of the folate−R67 DHFR complex, the edge of the pterin ring containing the O-4 and

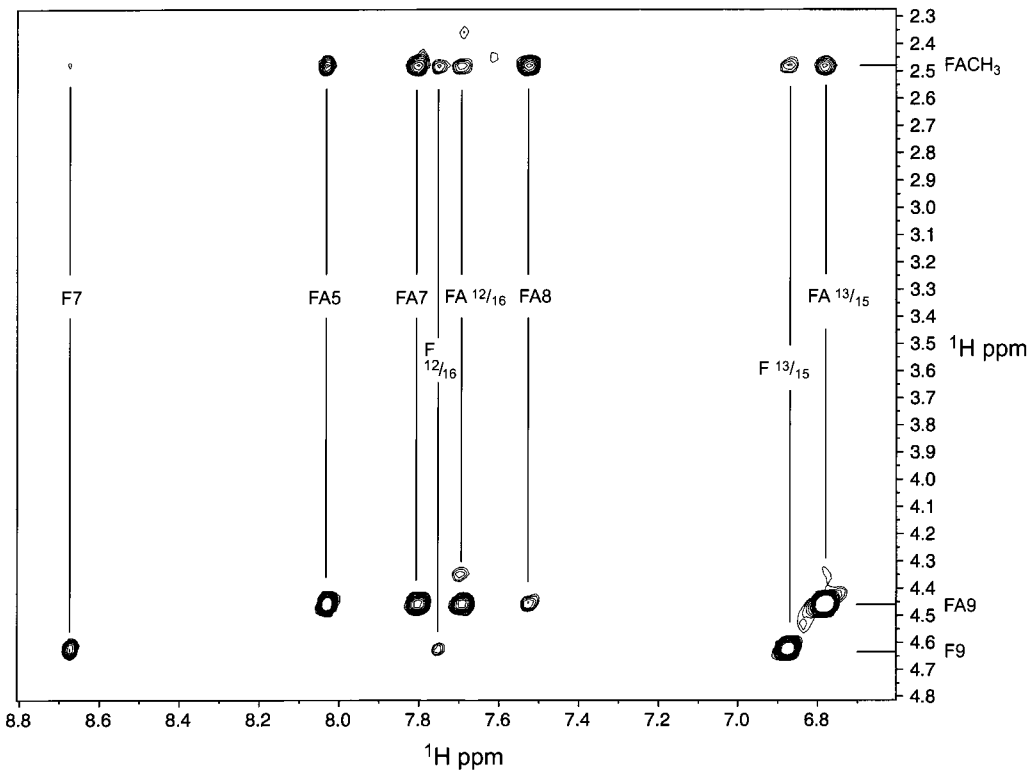

FIGURE 5: Portion of a NOESY spectrum showing the cross-peaks connecting methyl protons of DMDDF, and the H-9 protons of folate and DMDDF, with the aromatic protons in these molecules. The spectrum corresponds to a mixing time of 700 ms and was obtained at pH 9, 20 °C, in 100 mM Tris-d_{11} D_2O buffer. The positions of the DMDDF peaks are identified as FA for the folate analogue, while the corresponding folate protons are labeled with an F.

N-5 substituents for both folI and folII comes into close contact with the inside of the pore. Thus, changes in the folate−protein interaction resulting from the 5-deaza substitution probably contribute significantly to the observed differences. Unfortunately, NOESY studies performed on the $NADP^+$−8-deazafolate−R67 DHFR complex, which exhibits more favorable kinetic behavior than the $NADP^+$−DMDDF−DHFR complex, were of little additional value in elucidating the structure of the ternary complex since the H-7, H-8, and H12/16 protons (defined analogously to DMDDF, Figure 1) were not well resolved.

DISCUSSION

Despite the identity of the reactions catalyzed, type II DHFR adopts a unique structure that has little resemblance to chromosomal DHFR. The enzyme contains no separately evolved binding sites for substrate and cofactor, apparently following a "one site fits all" design. Additionally, the enzyme lacks the active site carboxyl group, which plays an important role in catalysis and forms the basis for the strong inhibition by aminopterin and diaminopyrimidine analogues (*23*−*25*). Indeed, catalysis presumably results primarily from the ability of the enzyme to correctly orient the $NADP^+$ and folate substrates for a sufficient time period to enable hydride transfer to occur. However, due to the symmetry of the enzyme and to the competition between $NADP^+$ and folate for binding to each half of the pore, a determination of the structure of the ternary complex represents a very challenging structural problem. The use of interligand Overhauser effects presents a potentially useful approach for dealing with this system. In the present study, we have been able to observe such effects for the $NADP^+$−folate/DMDDF−DHFR ternary complex, as well as for a ternary folate−DMDDF−DHFR complex, where DMDDF is an analogue of folate containing additional protons which can provide NOE information (Figure 1).

Table 2: Selected Internuclear Distances Corresponding to the Model of Ref *5* for a Ternary Ribonicotinamide−Methylpterin−DHFR Complex[a]

nicotinamide protons	folate nuclei					
	F7	C6	C9	F9	F9′	F9″
N2	6.13	5.67	4.91	**3.89**	5.03	5.59
N4	**3.49**	**3.19**	**3.84**	**3.41**	4.33	4.75
N5	**2.77**	4.06	4.54	**3.95**	5.47	4.97
N6	4.43	5.65	5.49	4.59	6.37	5.73

[a] Distances to folate protons correspond to folate 1 and are given in angstroms. Protons added to the structure using the program reduce (*27*). Distances under 4.0 Å are indicated in boldface.

Since there are relatively few NOEs which can be observed for the proton-poor pterin ring system, we have followed the approach of comparing the available data with previously discussed models, rather than trying to derive independent structures of the complexes. Narayana et al. (*5*) modeled the relative positions of the 6-methylpterin and ribonicotinamide based on the relative orientation observed for the chromosomal enzyme (*26*). Using the program reduce (*27*), we have introduced protons into the ligands and summarized some of the main interproton distances in Table 2. It is immediately apparent that there is a major discrepancy between the observed ILOE interactions and the interactions predicted from Table 2. In particular, the closest approach of protons from the two ligands based on the modeled complex is the 2.77 Å separation of N5 and F7 protons (Figure 6). However, we observed no ILOE connecting these protons. The next

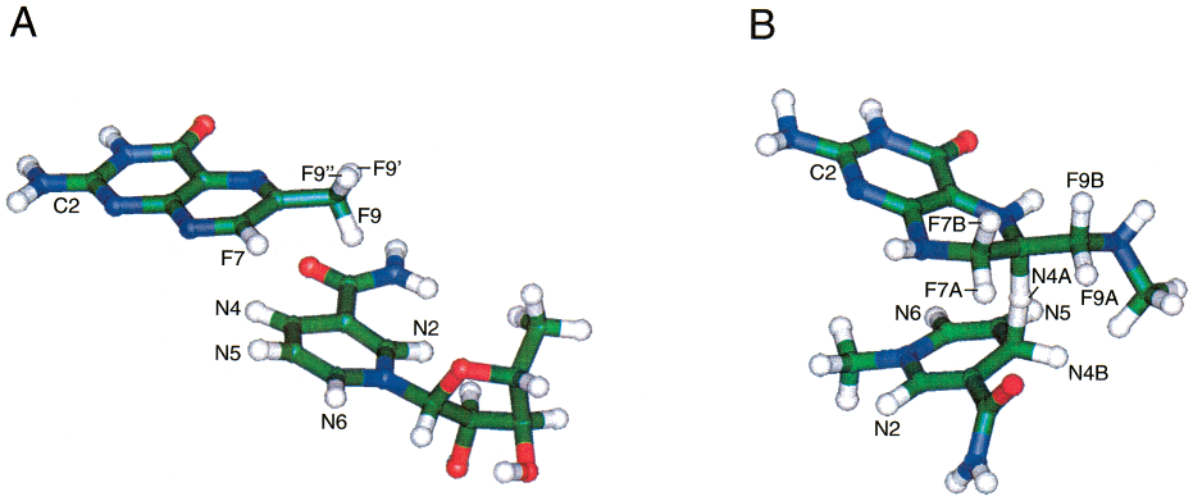

FIGURE 6: (A) Modeled orientation of 6-methylpterin and ribonicotinamide in the pore of R67 DHFR, derived from the data of Narayana et al. (*5*). In this figure, the central axis of the pore runs approximately from left to right, i.e., approximately parallel to the faces of the nicotinamide and pteridine ring systems. (B) Model of the DHFR transition state connecting reduced N-1 methyl nicotinamide and 6-methyl-7,8-dihydropterin analogue, calculated as described by Andres et al. (*28*).

most significant interactions, based on the interproton distances, are predicted to be $r_{N4-F9} = 3.41$ Å, $r_{N4-F7} = 3.49$ Å, $r_{N2-F9} = 3.89$ Å, and $r_{N5-F9} = 3.95$ Å, where we have given the values corresponding to the proton on the folate C9 closer to the nicotinamide ring. Again, the predicted ILOEs connecting N4 with F7 and N2 with F9 were not observed. In addition to these significant differences, the structure of the complex modeled by Narayana et al. (*5*) indicates the formation of a quaternary complex involving the DHFR and NADP(H) as well as two folate molecules, fol I and fol II (see Figure 4C and ref *5*), which is inconsistent with the isothermal titration calorimetry results of Bradrick et al. (*8*), which indicate only formation of ternary complexes. The modeled quaternary complex of Narayana et al. (*5*) implies a binding mode characterized by an orientation in which both cofactor and substrate lie next to each other on the same side of the central pore. Thus, the *p*-aminobenzoyl group of folate will be located close to the nicotinamide ring, and we would expect to see significant ILOE resonances connecting the corresponding protons. Weak ILOE peaks can be observed between the folate *p*-aminobenzoyl protons and nicotinamide N4; however, these exhibit a delayed buildup, suggesting that indirect relaxation pathways make significant contributions. Given the strong dipolar interaction between N4/5 and F9 and the strong F9−F12/16/13/15 transferred NOE peaks, such an indirect relaxation effect is very reasonable.

In contrast with the above model, Andres et al. (*28*) have computed a theoretical transition state complex for the reduction of dihydrofolate by NADPH which is characterized by an endo geometry in which the pyridine ring essentially eclipses the pterin ring 2 (Figure 6B). In this structure, the distance between nicotinamide C4 and folate C6 is 2.87 Å, and the rings tilt away from each other, so that the distance between the nicotinamide N1 and folate C8a is 4.26 Å (Figure 6B, Table 3). The relative orientation of substrate and cofactor calculated in this way thus differs dramatically from the orientation characterizing the chromosomal enzyme. Approximating the N4 proton position of $NADP^+$ by N4B in the transition structure (Figure 6), and the folate F7 proton position by F7A in the dihydrofolate, we see that $r_{N4B-F9A} = 3.29$ Å $< r_{N4B-F7A} = 3.75$ Å $< r_{N5-F9A} = 4.89$ A. This model is qualitatively more consistent with observed ILOE data obtained from the $NADP^+$−folate−DHFR complex. In this structure, the nicotinamide C3 position rather than the C5 position comes closest to F7, thus explaining the reduced NOE interactions between N5 and F7. Interestingly, the ribonicotinamide syn conformation demonstrated in the previous transferred NOE study by Brito et al. (*19*) on the related R388 DHFR similarly led to a model in which the nicotinamide C3 position rather than the C5 position comes closest to F7 (Figure 7B of ref *19*), also consistent with the present interligand NOE data.

Table 3: Internuclear Distances Corresponding to the Transition State Model of Ref *28*[a]

nicotinamide protons	folate nuclei				
	F2 amino-N	F7A	F7B	F9A	F9B
N2	7.05	4.36	5.81	6.15	7.12
N4B	8.51	**3.75**	4.90	**3.29**	4.49
N4A	6.94	**2.50**	**3.31**	**2.57**	**3.29**
N5	7.59	5.19	5.85	4.89	5.33
N6	6.41	6.04	6.74	6.68	6.99

[a] Distances are given in angstroms and distances under 4.0 Å are indicated in boldface. N4A is the hydride ion transferred between the reactants. N4B and F7A more closely approximate the positions of oxidizied nicotinamide N4 and folate F7.

Considering next the data obtained for the ternary $NADP^+$−DMDDF−DHFR complex, a model which places N4 near FA9 as required by the N4−FA9 ILOE data, and which places the methyl group FA2 in the vicinity of the ribonicotinamide protons as indicated by the data of Figure 4, immediately leads to a structure which is qualitatively similar to the transition state of Andres et al. (*28*) shown in Figure 6B. A typical structure modeled subject to these distance constraints is shown in Figure 7. Some of the relevant internuclear distances in this model are $r_{N6-N1'} = 2.39$ Å, $r_{N2-N2'} = 2.26$ Å, $r_{N4-FA9} = 3.72$ Å (closer proton), and $r_{N5-FA9} = 5.20$ Å (closer proton). The model is generally consistent with the other ILOE data in Table 1. In particular, the nicotinamide N4, N5, and N6 protons lie closest to FA5, although in the model the FA5 proton is closer to N4 than to N6. The carboxamide group of the nicotinamide is closest

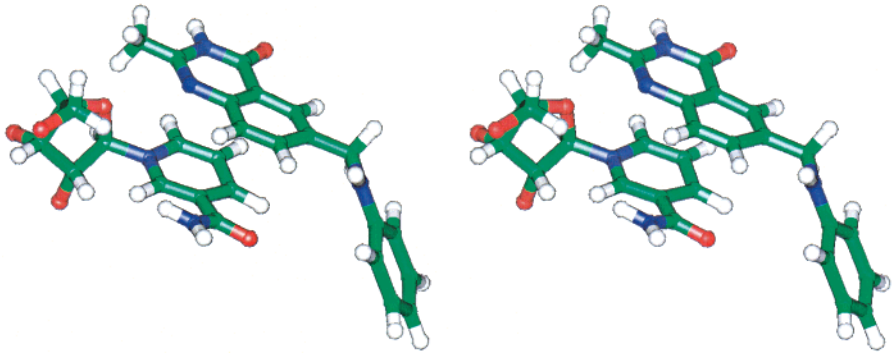

FIGURE 7: Stereopair for a model of the relative orientation of oxidized ribonicotinamide and DMDDF (with the *p*-aminobenzoyl glutamate replaced by aniline). The model is based on the ILOE data obtained and on the transition state structure shown in Figure 6B.

to FA7 and FA8, explaining the lower ILOEs to these protons. The distances of the methyl carbon of DMDDF to the ribonicotinamide NC5′ and to nicotinamide N2 proton in the model are 3.20 and 4.98 Å, respectively, consistent with the ILOE peaks seen in Figure 4. Hence we believe that this type of model provides a reasonable description for the predominant ternary complex formed from R67 DHFR, $NADP^+$, and DMDDF.

As noted in the previous section, the available NOE data support the conclusion that the $NADP^+$ adopts a similar conformation in the ternary complexes with both folate and DMDDF, indicating that this is a relevant structure for the true catalytic complex. Further, the nicotinamide adopts the same high syn geometry determined previously in the binary complex with the related R388 plasmid DHFR. Analogous with the results of Brito et al. (*19*), we similarly observed no NOEs connecting the adenine and nicotinamide ring systems, supporting the conclusion that the $NADP^+$ adopts an extended rather than a folded conformation when bound to the enzyme. We note, however, that in the present studies we did not observe the time-dependent changes in the spectra reported by Brito et al. (*7*), the basis of which remains undetermined. Additionally, no ILOE cross-peaks connecting the adenine protons with folate protons, which could arise from nonproductive complexes, were observed.

A strong although imperfect correlation exists between the ribonicotinamide glycosidic bond angle and the stereospecificity of hydride transfer in pyridine nucleotide-dependent redox enzymes (*29*−*31*). As a general rule, dehydrogenases which are A-side specific, i.e., transfer the nicotinamide *pro-R* hydrogen, typically bind the coenzyme in an anti conformation of the NMN moiety. The chromosomal DHFR falls into this category, transferring the *pro-R* hydrogen from NADPH and adopting an anti conformation about both of the glycosidic bonds of NADPH (*6*). Brito et al. (*7*) have shown that the type II R388 DHFR also transfers the *pro-R* hydrogen of NADPH, while in the binary complex the NADPH was observed to adopt a syn conformation for the glycosidic bond of the NMN moiety (*19*). The present observations indicate that this syn glycosidic bond conformation is preserved in the ternary $NADP^+$−folate−DHFR ternary complex. Hence, the type II DHFR represents an exception to the generality cited above. Possibly, a more complex correlation relating the stereochemistry of hydride transfer, glycosidic bond angle, and substrate/cofactor orientation can be derived, e.g., *pro-R*/syn/endo vs *pro-R*/anti/exo. Additional data will be required for such an evaluation.

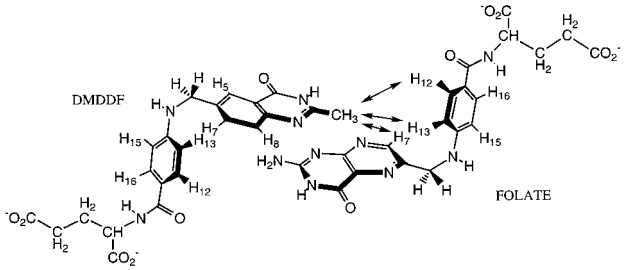

FIGURE 8: Schematic illustration of the ternary complex formed between folate, DMDDF, and DHFR. The NOE interactions between the C-2 methyl group of DMDDF and the protons of folate seen in Figure 4 are indicated by double-headed arrows. From the NOE data, the terminal glutamyl groups have increased mobility relative to the other portions of the molecules.

The stereochemistry of hydride transfer also has been the object of many theoretical calculations. Early calculations all indicated that optimal hydride transfer follows a linear path, so that the C···H···C bond angle is approximately 180° (*32*−*34*). However, most subsequent calculations using models more appropriate to the transfer of hydride ions from pyridine nucleotides to ring systems have found that a stacking geometry in which the pyridine and acceptor rings are described as "syn" or "endo" and the C···H···C bond is noticeably bent is in fact more optimal (*28*, *35*, *36*). Based on such calculations, the geometry of the ternary complex, which approximates the calculation of Andres et al. (*28*), may actually be more optimal than the structure adopted by the chromosomal enzyme. In fact, the most recent studies of Domingo and co-workers indicate that energy differences in the endo and exo transition state geometries are small enough so that the enzyme can utilize a geometry which is not completely dominated by the transition state energy but which presumably satisfies other constraints (*37*). The fact that type I and type II DHFRs apparently adopt very different ternary complex geometries supports this conclusion.

A schematic illustration of the ternary folate−DMDDF−DHFR structure qualitatively consistent with the ILOEs shown in Figure 5 is illustrated in Figure 8. This complex is structurally analogous to the ternary $(folate)_2$−DHFR complex shown in Figure 4C of ref *5*. Taking the coordinates from Narayana et al. (*5*) and adding the protons with the program reduce (*27*), we find r(fol I N2−fol II H7) = 4.75 Å and r(fol II N2−fol I H7) = 4.37 Å. The difference between these two distances reflects the fact that fol I and fol II in this structure are not symmetrically situated in the enzyme. These distances are shorter than the value of 6.6 Å

given in Table 1. This difference could arise from many factors, for example, normalization problems reflecting the mixture of $(folate)_2$−DHFR, folate−DMDDF−DHFR, and $(DMDDF)_2$−DHFR species present, so the consistency of these results is probably not unreasonable. The observed ILOE interactions between FA2 and the folate *p*-aminobenzoyl protons probably reflect a bent conformation of the folate molecule, as illustrated schematically in Figure 8.

In summary, the ILOE data appear to be consistent with the binding stoichiometry and the observation of NADP(H)−folate−DHFR, $(folate)_2$−DHFR, and $(NADPH)_2$−DHFR ternary complexes (*8*). The formation of these complexes predict that each half pore is capable of binding either substrate or cofactor. These previous ITC results in combination with the ILOE data indicate that pairs of ligands bind such that the bulk of the ligands and the negatively charged groups are located on opposite sides of the central pore, with the interacting aromatic systems, nicotinamide and/or pterins, in close contact at the center. This leads to a model in which a pair of folate or folate−DMDDF molecules would adopt a structure which is qualitatively similar to the proposed oligmers which can form in solution, with the ring systems stacked and the glutamyl groups of adjacent folate molecules pointing away from each other. For the ternary $NADP^+$−folate/DMDDF−DHFR complex, it is clear from the ILOE data that the relative orientation of the pyridine and pterin rings must differ significantly from their relative orientation in the chromosomal enzyme. A model closer to the endo transition state geometry derived by Andres et al. (*28*) for analogues in the gas phase is in much better qualitative agreement with the observed ILOE data. The transferred NOE data also support binding of the $NADP^+$ in an extended form, with a syn geometry for the ribonicotinamide and an anti geometry for the adenosine group, identical to previous conclusions derived from transferred NOE studies on the binary complex of $NADP^+$ with type II R388 DHFR (*19*). Analogous to the folate−DMDDF−DHFR ternary complex, the $NADP^+$−folate/DMDDF−DHFR ternary complex similarly involves extended folate and $NADP^+$ molecules which bind to opposite sides of the central pore, achieving some degree of overlap of the nicotinamide and pterin ring systems in the center. A ring stacking interaction may explain some of the positive cooperativity observed for dihydrofolate−$NADP^+$ binding (*8*). Unfortunately, there are too few NOE values at this point to allow determination of a more detailed structural model for this complex. It is anticipated that additional studies with other folate and $NADP^+$ analogues currently in progress will ultimately provide this information.

ACKNOWLEDGMENT

The authors are grateful to Prof. Luis Domingo for providing the coordinates to the transition state complex presented in ref *26*, to Robert Bass and Joseph Krahn for help with the modeling, and to Dr. Ray Blakley for helpful discussions.

REFERENCES

1. Fleming, M. P., Datta, N., and Gruneberg, R. N. (1972) Trimethoprim resistance determined by R factors, *Br. Med. J. 1*, 726−728.
2. Pattishall, K. H., Acar, J., Burchall, J. J., Goldstein, F. W., and Harvey, R. J. (1977) Two distinct types of trimethoprim-resistant dihydrofolate reductase specified by R-plasmids of different compatibility groups, *J. Biol. Chem. 252*, 2319−2323.
3. Smith, S. L., Stone, D., Novak, P., Baccanari, D. P., and Burchall, J. J. (1979) R plasmid dihydrofolate reductase with subunit structure, *J. Biol. Chem. 254*, 6222−6225.
4. Stone, D., and Smith, S. L. (1979) The amino acid sequence of the trimethoprim-resistant dihydrofolate reductase specified in *Escherichia coli* by R-plasmid R67, *J. Biol. Chem. 254*, 10857−10861.
5. Narayana, N., Matthews, D. A., Howell, E. E., and Xuong, N.-H. (1995) A plasmid-encoded dihydrofolate reductase from trimethoprim-resistant bacteria has a novel D2-symmetric active site, *Nat. Struct. Biol. 2*, 1018−1025.
6. Charlton, P. Q., Young, D. W., Birdsall, B., Feeney, J., and Roberts, G. C. K. (1979) Stereochemistry of Reduction of Folic Acid using Dihydrofolate Reductase, *J. Chem. Soc., Chem. Commun.*, 922−924.
7. Brito, R. M. M., Reddick, R., Bennett, G. N., Rudolph, F. B., and Rosevear, P. R. (1990) Characterization and stereochemistry of a cofactor oxidation by a Type II Dihydrofolate Reductase, *Biochemistry 29*, 9825−9831.
8. Bradrick, T. D., Beechem, J. M., and Howell, E. E. (1996) Unusual binding stoichiometries and cooperativity are observed during binary and ternary complex formation in the single active pore of R67 dihydrofolate reductase, a D2 symmetric protein, *Biochemistry 35*, 11414−11424.
9. Barsukov, I. L., Lian, L. Y., Ellis, J., Sze, K. H., Shaw, W. V., and Roberts, G. C. K. (1996) The conformation of coenzyme A bound to chloramphenicol acetyltransferase determined by transferred NOE experiments, *J. Mol. Biol. 262*, 543−558.
10. Li, D., DeRose, E. F., and London, R. E. (1999) The Inter-Ligand Overhauser Effect: A Powerful New NMR Approach for Mapping Structural Relationships of Macromolecular Ligands, *J. Biomol. NMR 15*, 71−76.
11. London, R. E. (1999) Theoretical Analysis of the Inter-Ligand Overhauser Effect, A New Approach for Mapping Structural Relationships of Macromolecular Ligands, *J. Magn. Reson. 141*, 301−311.
12. Reece, L. J., Nichols, R., Ogden, R. C., and Howell, E. E. (1991) Construction of a synthetic gene for an R-plasmid encoded dihydrofolate reductase and studies on the role of the N-terminus in the protein, *Biochemistry 30*, 10895−10904.
13. Hughes, L. R., Jackman, A. L., Oldfield, J., Smith, R. C., Burrows, K. D., Marsham, P. R., Bishop, J. A. M., Jones, T. R., O'Connor, B. M., and Calvert, A. H. (1990) Quinazoline antifolate thymidylate synthase inhibitors: alkyl, substituted alkyl, and aryl substituents in the C2 position, *J. Med. Chem. 33*, 3060−3067.
14. Sen, A. B., and Gupta, S. K. (1962) Possible antiamoebic agents. Part XVIII. Mannich Base Dihydrochlorides of substituted quinazolines, *J. Indian Chem. Soc. 39*, 368−372.
15. Marion, D., Ikura, M., Tschudin, R., and Bax, A. (1989) Rapid recording of 2D NMR spectra without phase cycling. Application to the study of hydrogen exchange in proteins, *J. Magn. Reson. 85*, 393−399.
16. Delaglio, F., Grzeseik, S., Vuister, G. W., Zhu, G., Pfeifer, J., and Bax, A. (1995) NMRPipe: a multidimesional spectral processing system based on UNIX pipes, *J. Biomol. NMR 6*, 277−293.
17. Goddard, D., and Kneller, D. G. SPARKY 3, University of California, San Francisco.
18. Nichols, R., Weaver, C. D., Eisenstein, E., Blakley, R. L., Appleman, J., Huang, T. H., Huang, F. Y., and Howell, E. E. (1993) Titration of Histidine 62 in R67 Dihydrofolate Reductase Is Linked to a Tetramer ↔ Two-Dimer Equilibrium, *Biochemistry 32*, 1695−1706.
19. Brito, R. M. M., Rudolph, F. B., and Rosevear, P. R. (1991) Conformation of $NADP^+$ Bound to a Type II Dihydrofolate Reductase, *Biochemistry 30*, 1461−1469.
20. Lam, Y. F., and Kotowycz, G. (1972) Self-association of folic acid in aqueous solution by proton magnetic resonance, *Can. J. Chem. 50*, 2357−2363.

21. Poe, M. (1978) Proton magnetic resonance studies of folate, dihydrofolate and methotrexate. Evidence from pH and concentration studies for dimerization, *J. Biol. Chem. 248*, 7025−7032.
22. Burch, H. B., Bradley, M. E., and Lowry, O. H. (1967) The measurement of triphosphopyridine nucleotide and reduced triphosphopyridine nucleotide and the role of hemoglobin in producing erroneous triphosphopyridine nucleotide values, *J. Biol. Chem. 242*, 4546−4554.
23. Cocco, L., Temple, C., Jr., Montgomery, J. A., London, R. E., and Blakley, R. L. (1981) Protonation of methotrexate bound to the catalytic site of dihydrofolate reductase from *Lactobacillus casei*, *Biochem. Biophys. Res. Commun. 100*, 413−419.
24. Cocco, L., Groff, J. P., Temple, C., Jr., Montgomery, J. A., London, R. E., Matwiyoff, N. A., and Blakley, R. L. (1981) Carbon-13 nuclear magnetic resonance study of protonation of methotrexate and aminopterin bound to dihydrofolate reductase, *Biochemistry 20*, 3972−3978.
25. Cocco, L., Roth, B., Temple, C., Jr., Montgomery, J. A., London, R. E. and Blakley, R. L. (1983) Protonated state of methotrexate, trimethoprim and pyrimethamine bound to dihydrofolate reductase, *Arch. Biochem. Biophys. 226*, 567−577.
26. Bystroff, C., Oatley, S. J., and Kraut, J. (1990) Crystal Structures of *Escherichia coli* Dihdyrofolate Reductase: The $NADP^+$ Holoenzyme and the Folate-$NADP^+$ Ternary Complex. Substrate Binding and a Model for the Transition State, *Biochemistry 29*, 3263−3277.
27. Word, J. M., Lovell, S. C., Richardson, J. S., and Richardson D. C. (1999) Asparagine and glutamine: Using hydrogen atom contacts in the choice of side-chain amide orientation, *J. Mol. Biol. 285*, 1735−1747.
28. Andres, J., Moliner, V., Safont, V. S., Domingo, L. R., Picher, M. T., and Krechl, J. (1996) On Transition Structures for Hydride Transfer Step: A Theoretical Study of the Reaction Catalyzed by Dihydrofolate Reducase Enzyme, *Bioorg. Chem. 24*, 10−18.
29. Benner, S. A. (1982) The stereoselectivity of alcohol dehydrogenases: a stereochemical imperative?, *Experientia 38*, 633−636.
30. Levy, H. R., Ejchart, A., and Levy, G. C. (1983) Conformations of Nicotinamide Coenzymes Bound to Dehydrogenases Determined by Transferred Nuclear Overhauser Effects, *Biochemistry 22*, 2792−2796.
31. You, K. S. (1985) Stereospecificity for nicotinamide nucleotides in enzymatic and chemical hydride transfer reactions, *Crit. Rev. Biochem. 17*, 313−451.
32. Donkersloot, M. C. A., and Buck, H. M. (1981) The Hydride-Donation Reaction of Reduced Nicotinamide Adenine Dinucleotide. 1. MINDO/3 and STO-3G Calculations on Analogue Reactions with Cyclopropene, Tropilidene, and 1,4-Dihydropyridine as Hydride Donors and the Cyclopropenium Cation as Acceptor, *J. Am. Chem. Soc. 103*, 6549−6554.
33. Van der Kerk, S. M., Van Gerresheim, W., and Verhoeven, J. W. (1984) Linear versus Bent Transition-state Structures in Hydride-Transfer Processes Mediated by NAD(P)H Model Systems−A Theoretical Investigation, *Recl. Trav. Chim. Pays-Bas 103*, 143−144.
34. De Kok, P. M. T., Donkersloot, M. C. A., van Lier, P. M., Meulendijks, G. H. W. M., Bastiaansen, L. A. M., Van Hooff, H. J. G., Kanters, J. A., and Buck, H. M. (1986) Stereoselective hydride Uptake in Model-Systems Related to the Redox-Couple NAD^+/NADH, *Tetrahedron 42*, 941−959.
35. Wu, Y.-D., and Houk, K. N. (1987) Theoretical Transition Structures for Hydride Transfer to Methyleniminium Ion from Methylamine and Dihydropyridine. On the Nonlinearity of Hydride Transfers, *J. Am. Chem. Soc. 109*, 226−227.
36. Wu, Y.-D., Lai, D. K. W., and Houk, K. N. (1995) Transition Structures of Hydride Transfer Reactions of Protonated Pyridinium Ion with 1,4-Dihydropyridine and Protonated Nicotinamide with 1,4-Dihydronicotinamide, *J. Am. Chem. Soc. 117*, 4100−4108.
37. Castillo, R., Andres, J., and Moliner, V. (1999) Catalytic mechanism of dihydrofolate reductase enzyme. A combined quantum-mechanical/molecular-mechanical characterization of transition state structure for the hydride transfer step, *J. Am. Chem. Soc. 121*, 12140−12147.

BI0026425